Acta Crystallographica Section A
Foundations and Advances
ISSN 2053-2733

Received 23 September 2013
Accepted 23 May 2014

A study of one-dimensional incommensurate modulated structure determination in high-resolution transmission electron microscopy

Xueming Li,‡ Binghui Ge, Fanghua Li,* Huiqian Luo and Haihu Wen¶

Beijing National Laboratory for Condensed Matter Physics, Institute of Physics, Chinese Academy of Sciences, PO 603, Beijing, 100190, People's Republic of China. Correspondence e-mail: lifh@iphy.ac.cn

The methods for determining incommensurate modulated structures (IMSs) in high-resolution transmission electron microscopy have been studied and improved to a level more perfect than before. This is demonstrated by means of the IMS determination for $Bi_{2.31}Sr_{1.69}CuO_{6+\delta}$ as an example. First, as previously, the projected potential map (PPM) of the IMS with resolution 0.2 nm was obtained after image deconvolution from a [100] image. Secondly, the resolution of the PPM was enhanced to 0.1 nm through phase extension combined with the electron-diffraction data so that the substitutional and displacive modulation functions could be determined. Thirdly, a (2+1)-dimensional structure model that corresponds to the [100] projected IMS was built for calculating the related partial structure factors that were utilized to correct the experimental electron-diffraction intensities for both main and satellite reflections. After three cycles of diffraction-intensity correction and phase extension, all unoverlapped atoms projected along the [100] direction in $Bi_{2.31}Sr_{1.69}CuO_{6+\delta}$ were resolved, and the modulations of substitution and displacement could be observed clearly. The substitution of Bi for Sr atoms at the Sr(O) columns was seen in the final PPM and verified by high-dimensional image simulation.

© 2014 International Union of Crystallography

1. Introduction

A structure is defined as a (3+1)-dimensional [(3+1)D] incommensurate modulated structure (IMS) when an additional modulation period exists apart from the three-dimensional (3D) fundamental lattice periods that describe the basic structure, and the ratio of the additional period to the corresponding period in the basic structure is irrational. For example, there are (3+2)- and (3+3)-dimensional IMSs. According to the physical mechanism, the modulation can be classified as a substitutional/compositional (or occupational) modulation, displacive modulation, magnetic modulation *etc.* (de Wolff, 1974).

The diffraction pattern of an IMS is composed of two kinds of reflections. The main reflections are situated on the three-dimensional fundamental lattice nodes, while the satellite reflections align symmetrically to every main reflection. Different from the three-dimensional periodic structures including superstructures, the triplet of ordinary indices h, k and l is insufficient to index all reflections for an IMS. The modulation wavevector $\mathbf{q}$ was proposed (de Wolff, 1974) as an additional component of the reciprocal-lattice vector $\mathbf{H}$ for a (3+1)D structure:

$$\mathbf{H} = h\mathbf{a}^* + k\mathbf{b}^* + l\mathbf{c}^* + m\mathbf{q}, \tag{1}$$

where h, k, l and m are integers, $\mathbf{a}^*$, $\mathbf{b}^*$ and $\mathbf{c}^*$ the reciprocal-basis vectors of the basic structure, and the modulation wavevector is expressed as $\mathbf{q} = \alpha\mathbf{a}^* + \beta\mathbf{b}^* + \gamma\mathbf{c}^*$ with at least one among α, β and γ being irrational.

X-ray (Leligny *et al.*, 1992; Rutzinger *et al.*, 2009; Wei *et al.*, 2011), neutron (Cheong *et al.*, 1991; Montanari *et al.*, 2005; Lazic *et al.*, 2008) and electron diffraction together with electron microscopy (Palatinus *et al.*, 2006; Withers *et al.*, 2010; Abakumov *et al.*, 2011; Boullay *et al.*, 2013) are traditional methods to study the IMS. Since high-resolution (HR) transmission electron microscopes can provide both electron-diffraction patterns and HR images, high-resolution transmission electron microscopy (HRTEM) has become an important tool to study structures and defects for crystals with a very small size. However, owing to the limited microscope resolution and lens aberrations, not all atoms can be distinguished in HR images, especially those that have a small atomic weight. There are two approaches to obtain the HR structural information by HRTEM. One is to take the images

‡ Present address: School of Life Sciences, Tsinghua University, Beijing, 100084, People's Republic of China.
¶ Present address: Physics School, Nanjing University, Nanjing, 210093, People's Republic of China.

nearby the Scherzer focus condition (Scherzer, 1949) with the microscope resolution improved by increasing the accelerating voltage of the microscope or using it with a Cs corrector. Another is to extract the HR information from the images recorded with a medium-voltage microscope by means of posterior image processing, such as exit-wave reconstruction (Schiske, 1968; Saxton, 1978; Kirkland, 1984; Kirkland *et al.*, 1985; Van Dyck *et al.*, 1996; Coene *et al.*, 1996) and electron-crystallography image processing (Li & Fan, 1979; Fan *et al.*, 1985; Han *et al.*, 1986; Hu & Li, 1991; Li, 2010; Kilaas *et al.*, 2005; Palatinus *et al.*, 2013; Willhammar *et al.*, 2012; Zou & Hovmöller, 2003).

The electron-crystallography image-processing method developed for *ab initio* crystal structure determination in our group contains two main steps: image deconvolution (Li & Fan, 1979; Han *et al.*, 1986; Hu & Li, 1991) and phase extension (Fan *et al.*, 1985). The term image deconvolution means to perform the operation inverse to the convolution to a single HR image and aims at deducting the effect of the contrast transfer function (CTF) so that the obtained deconvoluted image reflects directly the projected crystal structure. Hence, the deconvoluted image can be understood as the projected potential map (PPM), and the diffractogram obtained by Fourier transforming the deconvoluted image provides the low-resolution structure information including both amplitudes and phases of reflections with a resolution of about 0.2 nm. In combination with the electron-diffraction intensities that have a resolution of up to 0.1 nm or better, these low-resolution phases are used as the initial phases to derive the unknown phases of reflections with resolution in between 0.2 and 0.1 nm *via* the direct-methods phase extension developed in X-ray diffraction analysis. Then, an HR PPM, of resolution 0.1 nm or better, can be obtained by inversely Fourier transforming the final HR structural information including amplitudes and phases. This method was first applied to the *ab initio* structure determination of a $K_2O{\cdot}7Nb_2O_5$ crystal (Hu *et al.*, 1992).

In 1994, the phase-extension method developed for high-dimensional (HD) space (Hao *et al.*, 1987) was incorporated into electron-crystallographic image processing to study the (3+1)D structure of $Bi_2Sr_2CaCu_2O_x$ (Fu *et al.*, 1994). The observed image picked from the literature (Matsui & Horiuchi, 1988) was averaged according to the symmetry of the basic structure, and a PPM of the average structure of the IMS with a resolution of 0.17 nm was obtained after image deconvolution. The phases of main reflections with a resolution up to 0.17 nm were extracted from the Fourier transform of the PPM. Subsequently, the phases of main reflections with a resolution up to 0.1 nm were derived by phase extension. Then the phases of satellite reflections were derived *via* HD phase extension with all main reflection phases as the initial phases. Finally, an HR PPM of the IMS with a resolution of 0.1 nm was obtained by inversely Fourier transforming all main and satellite reflections (including both the amplitudes and the derived phases). This was the first IMS determined by the electron-crystallographic image-processing method. Later, the empirical method of electron-diffraction intensity correction that was first developed for the structure determination of three-dimensional periodic crystals and named the partial-structure-factor method (Huang *et al.*, 1996) was applied to the determination of the (3+1)D structure in $(Pb_{0.5}Sr_{0.3}Cu_{0.2})Sr_2(Ca_{0.6}Sr_{0.4})_2Cu_3O_y$ (hereafter named 'Pb'-1223) crystals (Liu *et al.*, 1998). In this case, only the main reflections were corrected by means of a partial structure model built based on the average structure map but the satellites were not corrected.

The two works (Fu *et al.*, 1994; Liu *et al.*, 1998) mentioned above made great strides in IMS determination in HRTEM, but there is still room for improvement. The present paper aims at developing further the approach to IMS determination, making it more quantitative and reliable than before.

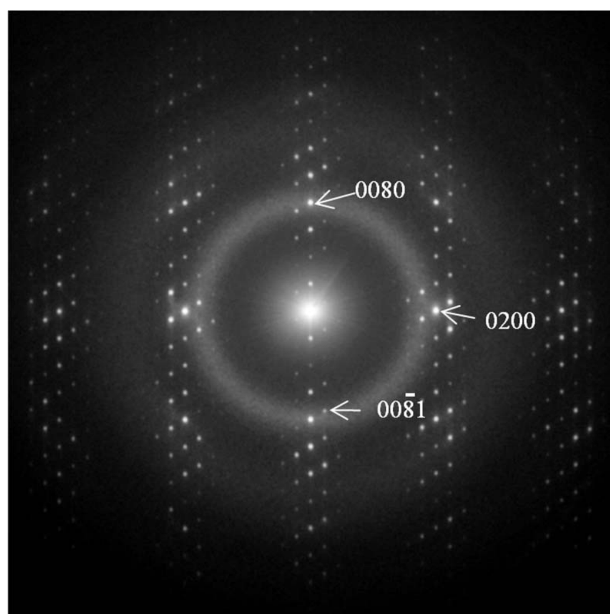

Figure 1
[100] electron-diffraction pattern of BSCO.

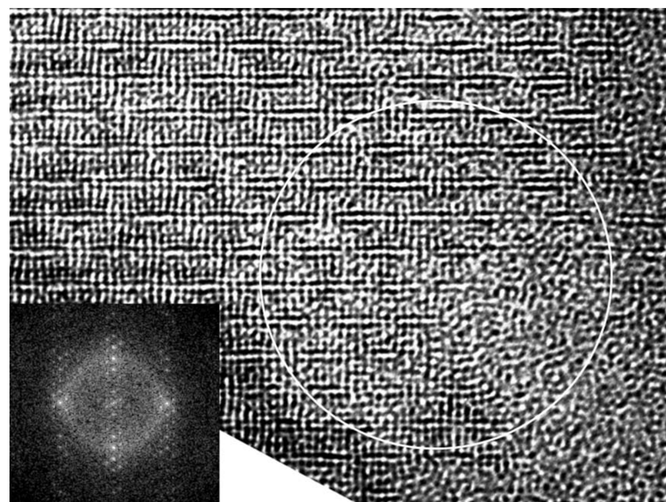

Figure 2
[100] HR image of BSCO and the diffractogram obtained from the circular region.

For this purpose the determination of the IMS in $Bi_{2.31}Sr_{1.69}CuO_{6+\delta}$ (BSCO) was chosen as an example to run the image-processing method, including previously and newly developed parts. The latter were focused on the derivation of atomic modulation functions and the contribution of partial IMS models for correcting both the main and satellite reflection intensities. In addition, the (3+1)D structural model used in HD multislice image simulation was improved by matching the observed image with a series of simulated images for different conditions.

2. Experimental methods

The single-crystal BSCO with nominal composition $Bi_{2.31}Sr_{1.69}CuO_{6+\delta}$ was prepared from mixed powders of Bi_2O_3, $SrCO_3$ and CuO by the travelling-solvent floating-zone technique (Luo *et al.*, 2007). Specimens for electron-microscope observation were first cut into thin slices from a bulk sample parallel to the (b, c) plane, and then the slices were thinned by mechanical polishing and ion milling. Because the BSCO slices are breakable, a sandwich sample was made by clamping the BSCO slice with two silicon wafers to prevent cleavage during mechanical polishing. The ion milling was performed by a Gatan PIPS 691 system. The specimens were observed with a Jeol 2010 HR electron microscope operated at 200 kV with point resolution about 0.2 nm. The diffraction patterns were recorded by DITABIS image plates and the HR images were recorded on electron-sensitive negative films and then digitized by corresponding scanners.

3. Image deconvolution and PPM of IMS with resolution 0.2 nm

Fig. 1 shows the [100] electron-diffraction pattern of BSCO. The satellites align from the bottom left to top right with the corresponding main reflections at the centre, indicating the existence of the (3+1)D structure. The lattice parameters of the basic structure were determined previously from the main reflections, and the modulation wavevector from both the main and satellite reflections. They are b = 0.543 nm, c = 2.453 nm and $\mathbf{q} = 0.223\mathbf{b}^* + 0.618\mathbf{c}^*$, where $\mathbf{b}^*$ and $\mathbf{c}^*$ are the reciprocal-basis vectors of the basic structure (Li *et al.*, 2009). The possible (3+1)D space groups determined previously are $B2/b(0\beta\gamma)$ and $Bb(0\beta\gamma)$ (Li *et al.*, 2009).

Fig. 2 is the [100] HR image corresponding to Fig. 1. The circular region is selected for performing the image processing. Its diffractogram inset in the bottom left of Fig. 2 is in agreement with the diffraction pattern shown in Fig. 1. After reducing the random noise by Fourier filtering, symmetry averaging was performed to correct the image distortion due to the crystal tilt and beam tilt. Because the symmetry-averaged images obtained from the two (3+1)D space groups are almost the same, only the one obtained with the group $B2/b(0\beta\gamma)$ and shown in Fig. 3(*a*) was used in the following. Fig. 3(*b*) is the image obtained by averaging Fig. 3(*a*)

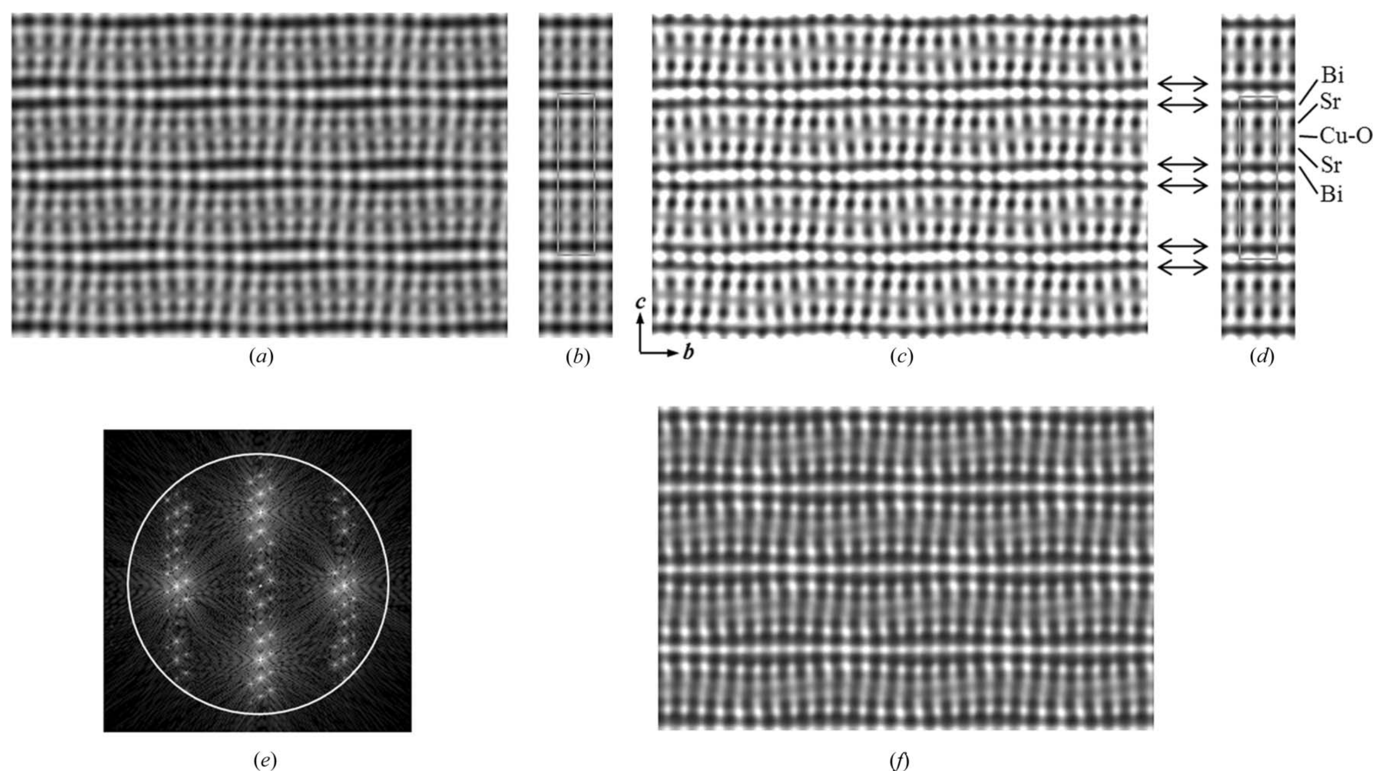

Figure 3
(*a*) Image obtained from the circular region given in Fig. 2 after Fourier filtering and high-dimensional symmetry averaging. (*b*) Average structure image corresponding to (*a*) and containing the information of main reflections only. (*c*), (*d*) Deconvoluted images corresponding to (*a*) and (*b*), respectively, with the arrows pointing to the Bi(O) atomic layers. (*e*) The diffractogram of (*c*) corresponding to the circle indicating the resolution 0.2 nm. (*f*) The [100] simulated image based on the parameters of modulation functions listed in Table 1.

Table 1
Parameters of modulation functions of BSCO corresponding to the (2+1)D structure model obtained from the [100] PPM shown in Fig. 7(*c*) and used to obtain the simulated image shown in Fig. 3(*f*).

$\bar{y}$ and $\bar{z}$ are average coordinates on the *b* and *c* axes, respectively, $\bar{p}$ is average occupancy. Δz and Δy are deviations of atomic position from the average position along the *b* and *c* axes, respectively, and Δp is deviation of occupancy from average occupancy. Deviations are expressed in the form of Fourier series $\Delta f(\tau) = \sum_n A_n \cos(2\pi\tau n) + B_n \sin(2\pi\tau n)$ ($f = y, z, p$).

Symmetry-independent atoms	Atomic average position and average occupancy		Parameters of modulation function: Deviation of atomic position and occupancy	Coefficient (n = 1, 2): A_1	B_1	A_2	B_2
Bi	$\bar{y}$	0.002	Δy	0.013	−0.051	−0.006	0.011
	$\bar{z}$	0.066	Δz	0.004	0.004	0.000	−0.001
	$\bar{p}$	0.900	Δp	0.109	0.043	−0.045	−0.017
Sr	$\bar{y}$	−0.006	Δy	0.033	−0.012	−0.003	−0.003
	$\bar{z}$	0.171	Δz	0.002	0.010	−0.001	0.001
	$\bar{p}$	1.02	Δp	−0.048	0.030	−0.009	0.002
Cu	$\bar{y}$	0.000	Δy	0.000	−0.006	0.000	0.002
	$\bar{z}$	0.250	Δz	0.000	0.012	0.000	0.002
	$\bar{p}$	1.0	Δp	0	0.000	0	0.000
O	$\bar{y}$	0.250	Δy	0.000	0.003	0.000	−0.002
	$\bar{z}$	0.250	Δz	0.000	0.014	0.000	0.001
	$\bar{p}$	1.0	Δp	0	0.000	0	0.000

according to the unit cell of the basic structure. Hereafter, such an image is named the average structure image. The structure information included in Fig. 3(*b*) corresponds to the main reflections only. The image defocus was determined from Fig. 3(*b*) by the method based on the principle of maximum entropy (Hu & Li, 1991). Two big peaks seen in the obtained entropy-defocus curve shown in Fig. 4 correspond to defocus values −37 and −65 nm. Considering the HR image was taken near the Scherzer focus (−41 nm), the correct defocus value should be −37 nm rather than −65 nm. The deconvoluted images corresponding to Figs. 3(*a*) and 3(*b*) were obtained and are shown in Figs. 3(*c*) and 3(*d*), respectively. Fig. 3(*c*) shows the [100] PPM of the IMS of resolution 0.2 nm with the black dots representing the projection of atomic columns, and Fig. 3(*d*) the [100] PPM of the average structure.

In comparison with the basic structure of BSCO (Torardi *et al.*, 1988), two adjacent rows of big black dots, marked by arrows in Figs. 3(*c*) and 3(*d*), should represent the Bi(O) atomic columns, and the other big black dots represent the Sr(O) atomic columns. The position and intensity fluctuations of the black dots seen in Fig. 3(*c*) indicate the existence of both displacive and substitutional modulations in BSCO. The image resolution of 0.2 nm is insufficient to resolve the atoms of Cu and O. In order to obtain the structure information in more detail, phase extension must be performed with the electron-diffraction intensities. This is described in the following section.

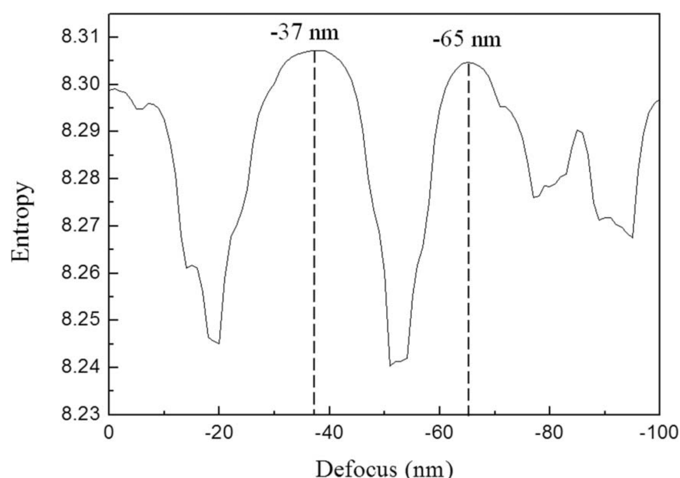

Figure 4
Entropy-defocus curve corresponding to Fig. 3(*c*).

4. Phase extension and PPM of IMS with resolution 0.1 nm

4.1. Preliminary PPM of resolution 0.1 nm

The phase extension was carried out as follows. First, the phases of 15 independent main reflections (hereafter all the main and satellite reflections means the independent ones) and 28 first-order satellite reflections within 0.2 nm resolution were extracted from the diffractogram (see Fig. 3*e*) obtained by Fourier transforming the PPM of the IMS shown in Fig. 3(*c*). These phases were used as the initial phases. Secondly, the intensities of 50 main reflections and 98 first-order satellites up to the resolution of 0.1 nm were measured from the [100] electron-diffraction pattern (Fig. 1), and the square roots of these intensities were treated approximately as the amplitudes of structure factors. Starting from the initial phases of resolution within 0.2 nm and the approximate amplitude up to the resolution 0.1 nm, HD phase extension was carried out to derive the unknown phases of main and satellite reflections within the resolution 0.1 nm. Finally, the information of main and satellite reflections (including both amplitudes and phases) was inversely Fourier transformed to obtain the PPM of the IMS with the resolution 0.1 nm as shown in Fig. 5(*a*). Fig. 5(*b*) is the [100] PPM of the average structure corresponding to Fig. 5(*a*). In comparison with Figs. 3(*c*) and 3(*d*),

the atomic columns are resolved more clearly, especially the Cu(O) and O columns in Figs. 5(*a*) and 5(*b*), but some atoms in Fig. 5(*a*) are still fuzzy, and some Sr(O) atomic columns show intensity that is unreasonably higher than that of the Bi ones. This is very probably due to the deviation of the observed diffraction intensity from the square structure factor. In order to improve the quality of the PPM, the diffraction intensity must be corrected.

4.2. Electron-diffraction intensity correction

4.2.1. A brief introduction to electron-diffraction intensity correction for three-dimensional periodic crystals. In practice, the observed diffraction intensities deviate from the ideal values owing to the Ewald sphere effect, dynamic scattering and other factors. An empirical method was proposed for offering a correction to the observed diffraction intensities such that the corrected intensities would approximate the square structure factors as much as possible (Huang *et al.*, 1996). To run the method a partial structure model is built based on part of the reliable structure information, for instance, the information on heavy atoms shown in the initial PPM, and the partial structure factors are calculated with this model. Then the diffraction intensities are corrected with the formula

$$I_c(\mathbf{H}) = \frac{\left\langle \left| F_p(\mathbf{H}) \right|^2 \right\rangle}{\left\langle I_0(\mathbf{H}) \right\rangle} I_0(\mathbf{H}), \qquad (2)$$

where $I_0(\mathbf{H})$ denotes the observed intensities, $I_c(\mathbf{H})$ the corrected intensities and $F_p(\mathbf{H})$ the partial structure factors. The fractional expression on the right-hand side of equation (2) represents the correction coefficient. The symbols $\langle\rangle$ denote averaging all reflections located inside a circular shell in the reciprocal space. In the PPM obtained by phase extension based on the corrected diffraction intensities the potential peaks would become sharper and some more atoms would appear. The second partial structure model would be built with the atoms that reasonably appeared added in, and used to run the next cycle of diffraction-intensity correction and phase extension. Such a procedure can be iteratively carried out until a satisfactory and stable PPM is obtained.

After applying this method, the strong observed diffraction intensities become even stronger and the weak ones even weaker. In addition, the reflections situated at the very low scattering angle region are weakened significantly. This means that the method is beneficial to reduce the dynamical scattering effect and compensate the effect of Ewald sphere curvature. It has been proved that the above-mentioned image-processing method is fruitful in the application to the *ab initio* structure determination of minute crystals (Lu *et al.*, 1997; Jiang *et al.*, 1999; Liu *et al.*, 2001; Wang *et al.*, 2002).

4.2.2. (2+1)D partial structure model. It was reported that the PPM of the IMS in 'Pb'-1223 (Liu *et al.*, 1998) was significantly improved even if only the main reflection intensities were corrected with a projected structure model built based on the average structure of the IMS. However, the uncorrected dynamical-diffraction effect in the satellite reflections may also lead to an obvious distortion in the resultant PPM when the incommensurate modulation is very strong. In addition, the amplitudes of partial structure factors calculated from the two-dimensional periodic model may be far from a good approximation to the kinematic amplitudes of main reflections. Hence, a (2+1)D partial structure model including the information of structural modulation becomes

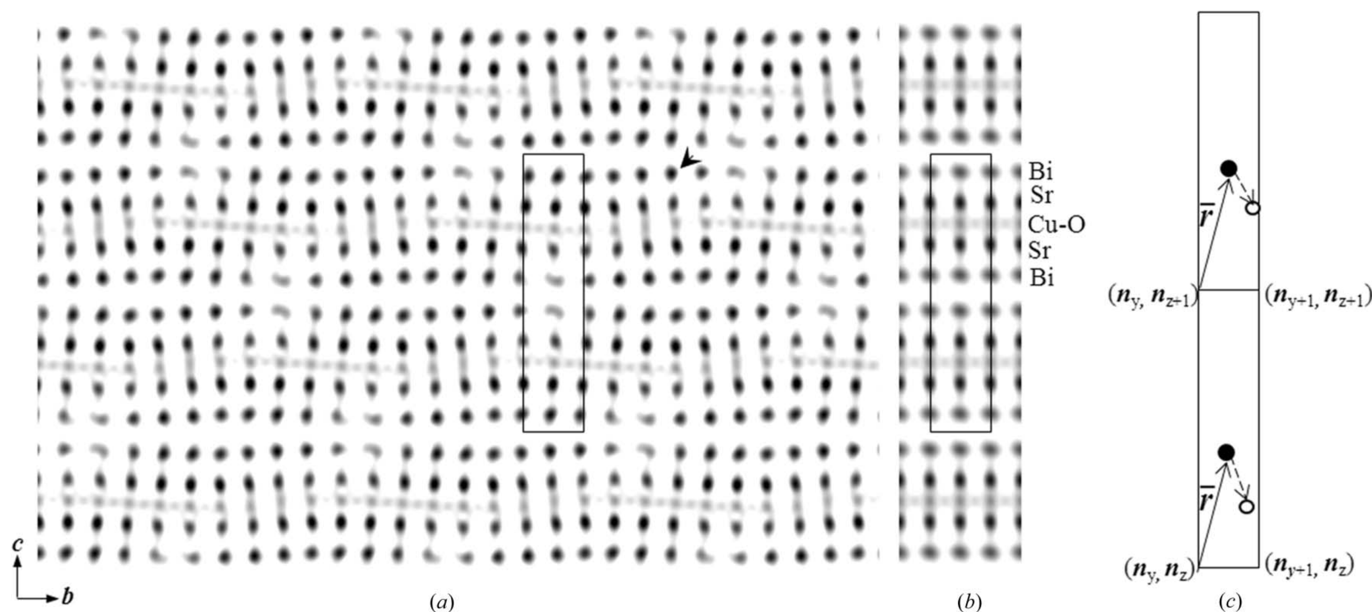

Figure 5
(*a*) [100] PPM of the IMS with resolution 0.1 nm obtained after phase extension based on the observed electron-diffraction data, and the dot marked by an arrow is considered to be fully occupied by Bi. (*b*) [100] PPM of the average structure corresponding to (*a*). (*c*) Schematic diagram showing the atomic positions $\bar{\mathbf{r}}$ and unit-cell origins $\mathbf{n}$ in the form of vectors in the average structure, and the open circle indicates an atom in the IMS, the solid circle an atom in the average structure corresponding to the open circle. The rectangles represent unit cells of the average structure.

necessary for the intensity correction. For this purpose, a new approach was developed to measure the structural modulation from the experimental image.

According to the HD space description (de Wolff, 1974), the (3+1)D structure can be described as a three-dimensional supersection obtained by cutting a (3+1)D periodic structure with the three-dimensional physical space. Principally, one may derive a (3+1)D structure model based on Fig. 5(*a*), utilize it as the partial structure model, calculate the partial structure factor for both the main and satellite reflections, and correct the diffraction intensities. However, in the present case, the preliminary [100] PPM of resolution 0.1 nm, in which most of the atomic columns are revealed (see Fig. 5*a*), was utilized directly as the partial IMS model to correct the intensities of the main and satellite reflections. Though the IMS is aperiodic in the physical space, it is possible to describe the [100] PPM of the IMS in BSCO shown in Fig. 5(*a*) as an artificial (2+1)D periodic structure, for which the two-dimensional periodic space corresponds to the (*b*, *c*) plane, while the additional one-dimensional space is perpendicular to and outside the physical space. The (2+1)D artificial structure model would serve as a tool to calculate the partial structure factor of the IMS and then correct the intensity of both main and satellite reflections. For this purpose, the modulation functions that carry the information of atomic position and occupancy in the (2+1)D space would be derived from a limited-size [100] PPM of the IMS (see Fig. 5*a*).

4.2.3. (2+1)D structural data set and modulation functions. Let $\mathbf{a}_1$, $\mathbf{a}_2$, $\mathbf{a}_3$, $\mathbf{a}_4$ and $\mathbf{b}_1$, $\mathbf{b}_2$, $\mathbf{b}_3$, $\mathbf{b}_4$ represent the basis vectors in the (3+1)D real space $\mathbf{R}_4$ and those in the corresponding reciprocal space, respectively, and the reciprocal-lattice vector $\hat{\mathbf{H}}$ can be expressed as

$$\hat{\mathbf{H}} = h_1\mathbf{b}_1 + h_2\mathbf{b}_2 + h_3\mathbf{b}_3 + h_4\mathbf{b}_4, \qquad (3)$$

with h_1, h_2, h_3 and h_4 being integers. The reciprocal-basis vectors are defined as $\mathbf{b}_1 = \mathbf{a}^*$, $\mathbf{b}_2 = \mathbf{b}^*$, $\mathbf{b}_3 = \mathbf{c}^*$, $\mathbf{b}_4 = \mathbf{q} + \mathbf{e}$, where $\mathbf{q} = \alpha\mathbf{a}^* + \beta\mathbf{b}^* + \gamma\mathbf{c}^*$ with at least one among α, β and γ being irrational, and $\mathbf{e}$ is a unit vector perpendicular to the physical space $\mathbf{R}_3$, *i.e.* the three-dimensional hyperplane in $\mathbf{R}_4$. According to the reciprocal relationship

$$\mathbf{a}_i \cdot \mathbf{b}_j = \begin{cases} 1 & i = j \\ 0 & i \neq j \end{cases},$$

the basis vectors in $\mathbf{R}_4$ are derived as

$$\mathbf{a}_1 = \mathbf{a} - \alpha\mathbf{e}, \quad \mathbf{a}_2 = \mathbf{b} - \beta\mathbf{e}, \quad \mathbf{a}_3 = \mathbf{c} - \gamma\mathbf{e}, \quad \mathbf{a}_4 = \mathbf{e}. \qquad (4)$$

Because $\mathbf{e}$ is perpendicular to $\mathbf{R}_3$, an arbitrary vector (x_1, x_2, x_3, x_4) located in $\mathbf{R}_3$ must obey

$$\mathbf{e}(x_1\mathbf{a}_1 + x_2\mathbf{a}_2 + x_3\mathbf{a}_3 + x_4\mathbf{a}_4) = 0, \qquad (5)$$

where x_1 to x_4 denote the fractional coordinates. Substituting the expression of $\mathbf{a}_1$, $\mathbf{a}_2$, $\mathbf{a}_3$ and $\mathbf{a}_4$ given in equation (4) for those included in equation (5), the fourth coordinate is derived as $x_4 = \alpha x_1 + \beta x_2 + \gamma x_3$. For the [100] PPM in BSCO $\alpha = 0$, then

$$x_4 = \beta x_2 + \gamma x_3. \qquad (6)$$

It is reasonable to assign x_2 and x_3 equal to the coordinates y and z in $\mathbf{R}_3$, respectively. Accordingly, x_4 is replaced by τ.

When the [100] projected average structure is concerned, equation (6) can be written as

$$\tau = \beta(\overline{y} + n_y) + \gamma(\overline{z} + n_z), \qquad (7)$$

where $\overline{y}$ and $\overline{z}$ are the fractional coordinates of an atom in the unit cell of average structure, and n_y and n_z coordinates of the corresponding unit-cell origin (see Figs. 5*b* and 5*c*). For simplicity, equation (7) is rewritten in the form of vectors

$$\tau = \mathbf{q} \cdot (\overline{\mathbf{r}} + \mathbf{n}), \qquad (8)$$

with $\overline{\mathbf{r}} = \overline{y}\mathbf{b} + \overline{z}\mathbf{c}$, $\mathbf{n} = n_y\mathbf{b} + n_z\mathbf{c}$. The schematic diagram illustrating the definition of $\overline{\mathbf{r}}$ and $\mathbf{n}$ is shown in Fig. 5(*c*). For a certain atom, $\overline{\mathbf{r}}$ is a constant and $\mathbf{n}$ is a variable changing with the position of the unit cell in the lattice of average structure.

The structural data of the (2+1)D structure mentioned above can be expressed as the set of average lattice coordinates $\overline{r}_j$ and average occupancies $\overline{p}_j$ measured from Fig. 5(*b*) together with the set of deviations $\Delta r_j = r_j - \overline{r}_j$ and $\Delta p_j = p_j - \overline{p}_j$, where j is the symbol of the jth atom in the average structure. In the following, the procedure of extracting the (2+1)D structural data set and determining the modulation functions of BSCO from a finite-sized PPM of the IMS will be given.

The average atomic positions $\overline{y}_j$ and $\overline{z}_j$ can be obtained directly by reading the coordinates of black dots inside the unit cell shown in Fig. 5(*b*), where each black dot represents an atom, and the average grey level was measured. As to converting the grey level of black dots into the average occupancy $\overline{p}_j$, first it is necessary to define the value of unit occupancy. For this purpose the Bi site with the strongest contrast as marked by an arrow (see Fig. 5*a*) was assumed to be fully occupied by a Bi atom and its grey level integrated within the ion radius of Bi atoms was treated as the unit occupancy. Then the average occupancy of Bi sites in Fig. 5(*b*) can be estimated by referring to the defined unit occupancy, and for Sr sites the ratio of atomic weights between Sr and Bi atoms was taken into consideration. Since, comparing with Bi and Sr, the smaller atomic number of Cu and O may lead to a larger error in the occupancy estimation, the substitutional modulations were ignored at this stage with the average occupations treated as unity for both Cu and O atoms. Accordingly, the values of y, z and p were measured for all black dots in Fig. 5(*a*) and their deviations from the average values, $\Delta y = y - \overline{y}$, $\Delta z = z - \overline{z}$ and $\Delta p = p - \overline{p}$, can be calculated. Obviously, the data set obtained is not perfect but contains a limited number of atoms only. The next step is to extend the data set infinitely in the (*b*, *c*) plane by deriving the modulation functions.

The procedure will be described in more detail for Bi atoms as an example. A two-dimensional lattice formed by $\mathbf{b}$ and $\mathbf{c}$, namely, the lattice for the [100] average structure, is superimposed on Fig. 5(*a*). The rectangle placed at the centre of Fig. 5(*a*) indicates a unit cell of the two-dimensional average lattice. Pick out all Bi atoms corresponding to the same average position $\overline{r}_j$, read their coordinates y and z, measure

their grey levels, record the corresponding unit-cell origin n, and calculate Δy, Δz and Δp. Because the (3+1)D atoms behave as strings having periodic bends or densification along $\mathbf{a}_4$ for displacive and substitutional modulations, respectively (de Wolff, 1974), the values of Δy, Δz and Δp should sit on a certain periodic curve, arranged in the order of the corresponding fourth coordinates. For simplicity, the values of the fourth coordinates were calculated only for the average structure. According to equations (7) or (8), each deviation of atomic position or occupancy can be expressed as a dual data set, for instance, $(\Delta y, \tau)$, ignoring the integer part in τ. Three sequences of discrete data points for Δy, Δz and Δp can be obtained by rearranging $(\Delta y, \tau)$, $(\Delta z, \tau)$ and $(\Delta p, \tau)$ in ascending order of τ.

The analytic expression of the modulation functions can be obtained by Fourier curve fitting to these sequences. Taking the case of Δy, the bilinear interpolation is used to get an equal interval array, then the array is fast Fourier transformed (FFT) to obtain the Fourier coefficients. In this work, the Fourier coefficients are expressed in the form of trigonometric functions, and the analytic modulation function is written as

$$\Delta y(\tau) = \sum_n A_n \cos(2\pi\tau n) + B_n \sin(2\pi\tau n).$$

Because the coefficients A_n and B_n decrease steeply with an increase of the order n, only the first two terms with $n = 1$ and 2 have been taken into consideration. The same method can be used to obtain the other analytical modulation functions $\Delta z(\tau)$ and $\Delta p(\tau)$ and for all atoms. Finally, the (2+1)D coordinates and occupancies of all atoms have been determined in the (2+1)D structure of BSCO, and the partial structure factors corresponding to the [100] PPM of BSCO have been calculated and utilized to correct the diffraction intensities. Although in the present case the modulation functions for all independent atoms have been obtained straightforwardly, for clarity the term 'partial structure factor' is used because it is calculated based on the rough structure model and used for intensity correction following the traditional partial-structure-factor method.

4.3. Improved PPM at 0.1 nm resolution

The [100] partial structure factors up to 0.1 nm resolution were calculated according to the (2+1)D structure model mentioned above. According to equation (2) the observed diffraction intensity has been corrected for all main and satellite reflections, and phase extension rerun with the square roots of corrected intensities as the amplitudes of the corresponding structure factors. Such correction and phase extension have been iteratively carried out until a reliable PPM is achieved. Fig. 6 shows a flow chart of the electron-crystallography image-processing method mentioned above.

Figs. 7(*a*) and 7(*b*) show the improved PPM at 0.1 nm resolution and the corresponding average structure after the first cycle of correction and phase extension, respectively. In comparison with Fig. 5(*a*), which was obtained with the diffraction intensities uncorrected, all atoms (black dots) in Fig. 7(*a*) become more convergent and, especially, the grey

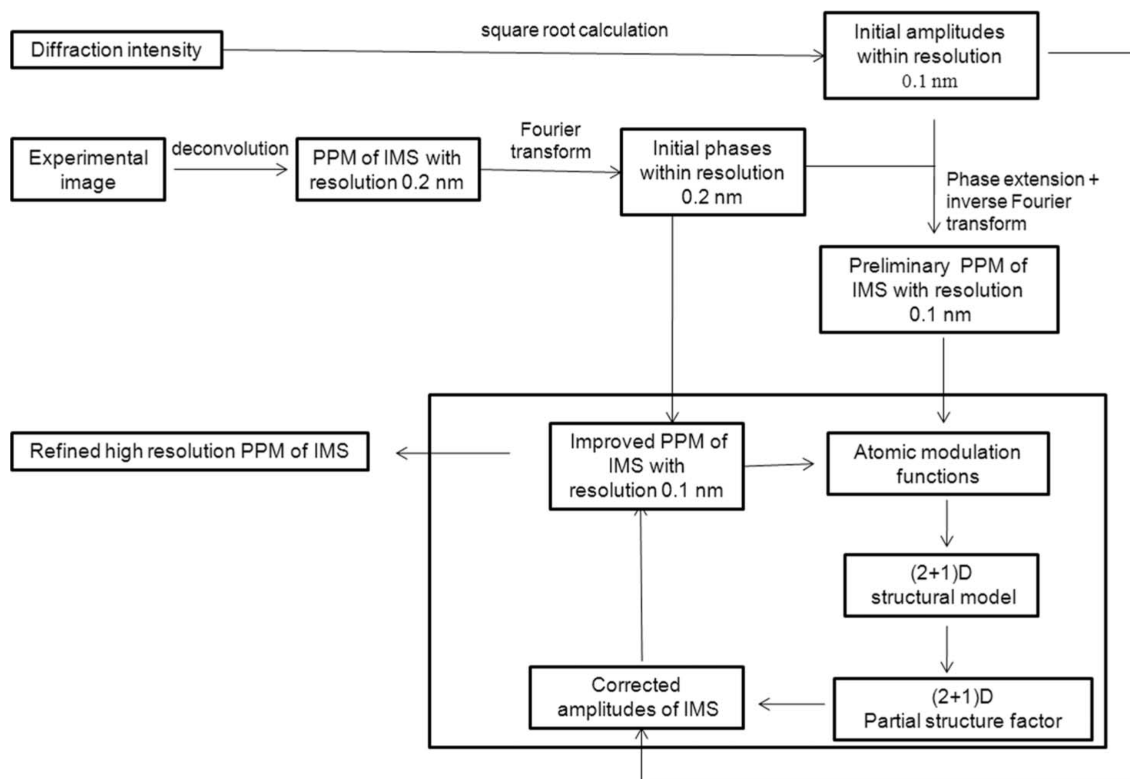

Figure 6
Flow chart of the present image-processing method; the part in the rectangle can be iteratively carried out until satisfactory results are obtained.

level for Sr sites becomes lower and reasonable. After three cycles of intensity correction and phase extension, the atoms have become even more convergent as shown in Figs. 7(*c*) and 7(*d*), and all artificial peaks appearing in Fig. 7(*a*) have vanished from sight (see Fig. 7*c*), and all the unoverlapped atomic columns projected along the [100] direction in BSCO, namely, Bi(O) and Sr(O), Cu(O) and O atoms, can be observed clearly.

4.4. Image simulation

The atomic coordinates can be quantitatively read out from the positions of black dots in the final [100] PPM shown in Fig. 7(*c*). However, the contrast of the black dots in the image is affected by the background subtraction and intensity scaling so that it is hard to precisely measure the absolute occupancy of the atoms as well as the ratio of substitutions among different atoms. Nevertheless, the question arises from the nominal chemical component of BSCO of whether some Sr sites may be occupied by Bi atoms. To answer the question, the Bi substitution at Sr sites has been semi-quantitatively estimated by HRTEM image simulation.

The multislice method has been applied to the [100] high-resolution image simulation for BSCO. The slice thickness is equal to the length of the *a* axis and all slices are identical to one another. The [100] projected structure of the slice is incommensurately modulated, because the modulation wavevector **q** is parallel to the slice plane. Therefore, the HD space description of the IMS has been implemented in the multislice simulation by means of the calculation procedure proposed by Sha *et al.* (1993).

The basic calculating procedures for the HD multislice simulation (Sha *et al.*, 1993) are similar to the three-dimensional case. The difference is mainly in the construction of a (2+1)D periodic structure by positioning main reflections and corresponding satellites into a (2+1)D array, and then the array is inversely Fourier transformed to obtain a (2+1)D transmission function of the IMS. Together with the propagation function revised in (2+1)D format, the *n*-beam dynamical calculations for a modulated structure divided into certain slices are carried out, following the conventional multislice method.

Based on the IMS model built from Fig. 7(*c*) and the HD multislice method, a series of HRTEM images are simulated with various defocus values, sample thickness and average occupancy (0.96–1.1) of the Sr site. The image similarity is quantified by the normalized cross-correlation coefficient

$$\frac{1}{N}\sum_{x,y}\frac{\left[I_1(x,y)-\overline{I}_1\right]\left[I_2(x,y)-\overline{I}_2\right]}{\sigma_1\sigma_2},$$

where N is the number of pixels, and $I_1(x, y)$ and $I_2(x, y)$ denote the pixel values in observed and simulated images, respectively, $\overline{I}_1$ and $\overline{I}_2$ the mean pixel values, σ_1 and σ_2 the standard deviations corresponding to $I_1(x, y)$ and $I_2(x, y)$, respectively. The best parameters fitting to the maximum cross-correlation value have been determined to be defocus value −41 nm, thickness 2.68 nm and average occupancy of Sr site 1.02. The corresponding simulated image is shown in Fig. 3(*f*). The excellent matching of Fig. 3(*f*) with the experimental image Fig. 3(*a*) verifies the above parameters. All the final parameters including modulation functions of Bi(O), Si(O), and Cu(O) and O are listed in Table 1. The maximum occupancy for Sr sites can go up to 1.08, which is larger than unity. On Sr sites, there are two candidates contributing to the occupancy fluctuation, Bi and O atoms overlapped with Sr atoms at Sr(O) columns. Considering that there is much less contrast of light O atoms

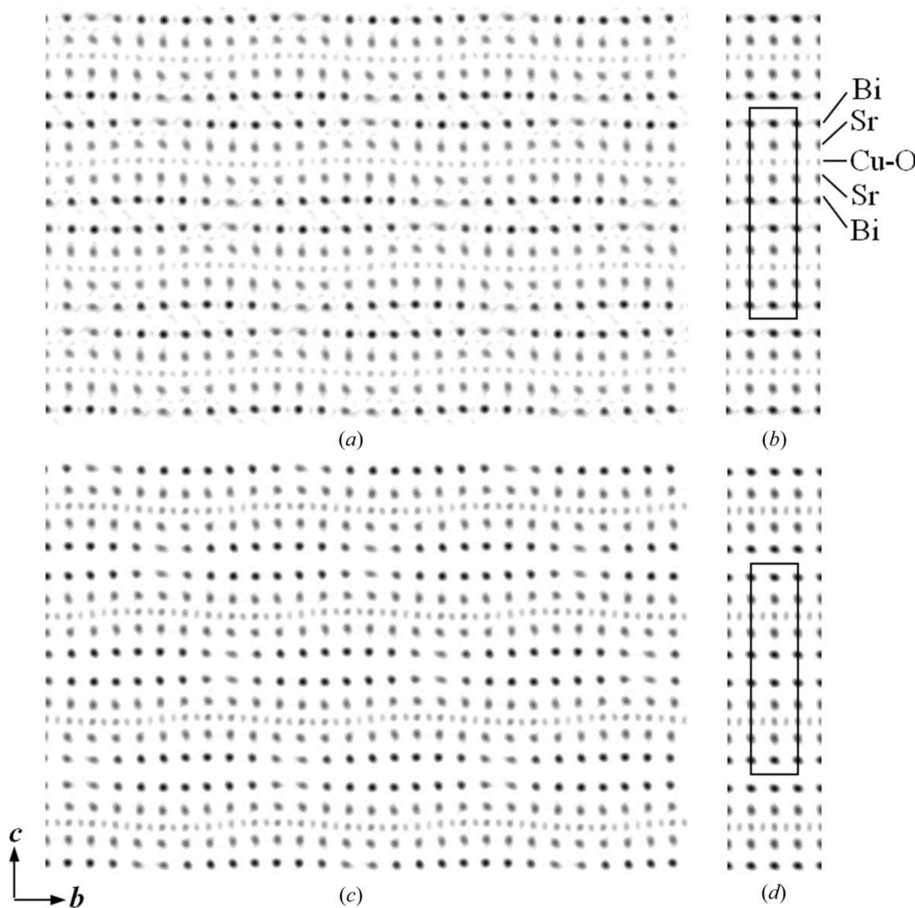

Figure 7
(*a*) [100] PPM of the IMS obtained after phase extension and the first cycle of diffraction-intensity correction. (*b*) PPM of average structure corresponding to (*a*). (*c*) [100] PPM of the IMS after phase extension and three cycles of diffraction-intensity correction. (*d*) PPM of average structure corresponding to (*c*). The frames in (*b*) and (*d*) denote the unit cell of the average structure.

than heavy Sr and Bi atoms, the contribution from O atoms should be very small. Therefore, the excess of ~8% Sr intensity indicates a high probability of the substitution of Bi for Sr atoms at the Sr(O) columns.

5. Conclusion

The (3+1)D structure in $Bi_{2.31}Sr_{1.69}CuO_{6+\delta}$ has been solved by electron-crystallographic image processing consisting of image deconvolution and phase extension in combination with the electron-diffraction data. An approach has been developed for the first time to determine the displacive and substitutional modulation functions from the obtained preliminary [100] PPM of the IMS at 0.1 nm resolution. This enables us to build an artificial (2+1)D periodic structure model for calculating the (2+1)D partial structure factors which we utilize to correct both the main and satellite reflection intensities. This means that the quality of the final [100] PPM is significantly improved so that the modulations of all unoverlapped atoms along the [100] direction are clearly visible. Moreover, by means of the HD multislice simulation the final IMS model, especially the substitution of Bi for Sr atoms at the Sr(O) columns, has been verified.

It is worth mentioning that the method utilized in this article to obtain the PPM of the IMS in BSCO at the resolution of 0.1 nm can be greatly simplified if the HR images are taken with aberration-corrected electron microscopes. The subject is under investigation and results will be published before long.

This work was supported by the National Basic Research Program of China (grant Nos. 2006CB601001 and 2011CBA001001) and the National Natural Science Foundation of China (grant Nos. 50672124, 10874207, 11104327 and 11374332).

References

Abakumov, A. M., Batuk, D., Hadermann, J., Rozova, M. G., Sheptyakov, D. V., Tsirlin, A. A., Niermann, D., Waschkowski, F., Hemberger, J., Van Tendeloo, G. & Antipov, E. V. (2011). *Chem. Mater.* **23**, 255–265.

Boullay, P., Palatinus, L. & Barrier, N. (2013). *Inorg. Chem.* **52**, 6127–6135.

Cheong, S. W., Aeppli, G., Mason, T., Mook, H., Hayden, S., Canfield, P., Fisk, Z., Clausen, K. & Martinez, J. (1991). *Phys. Rev. Lett.* **67**, 1791–1794.

Coene, W. M. J., Thust, A., deBeeck, M. & Van Dyck, D. (1996). *Ultramicroscopy*, **64**, 109–135.

Fan, H.-F., Zhong, Z.-Y., Zheng, C.-D. & Li, F.-H. (1985). *Acta Cryst.* A**41**, 163–165.

Fu, Z. Q., Huang, D. X., Li, F. H., Li, J. Q., Zhao, Z. X., Cheng, T. Z. & Fan, H. F. (1994). *Ultramicroscopy*, **54**, 229–236.

Han, F.-S., Fan, H.-F. & Li, F.-H. (1986). *Acta Cryst.* A**42**, 353–356.

Hao, Q., Liu, Y.-W. & Fan, H.-F. (1987). *Acta Cryst.* A**43**, 820–824.

Hu, J. J. & Li, F. H. (1991). *Ultramicroscopy*, **35**, 339–350.

Hu, J. J., Li, F. H. & Fan, H. F. (1992). *Ultramicroscopy*, **41**, 387–397.

Huang, D. X., Liu, W., Gu, Y. X., Xiong, J. W., Fan, H. F. & Li, F. H. (1996). *Acta Cryst.* A**52**, 152–157.

Jiang, H., Li, F. H. & Mao, Z. Q. (1999). *Micron*, **30**, 417–424.

Kilaas, R., Marks, L. D. & Own, C. S. (2005). *Ultramicroscopy*, **102**, 233–237.

Kirkland, E. J. (1984). *Ultramicroscopy*, **15**, 151–172.

Kirkland, E. J., Siegel, B. M., Uyeda, N. & Fujiyoshi, Y. (1985). *Ultramicroscopy*, **17**, 87–103.

Lazic, B., Krüger, H., Kahlenberg, V., Konzett, J. & Kaindl, R. (2008). *Acta Cryst.* B**64**, 417–425.

Leligny, H., Durčok, S., Labbe, P., Ledesert, M. & Raveau, B. (1992). *Acta Cryst.* B**48**, 407–418.

Li, F. H. (2010). *Phys. Status Solidi A*, **207**, 2639–2665.

Li, F. H. & Fan, H. F. (1979). *Acta Phys. Sin.* **2**, 276–278.

Li, X. M., Li, F. H., Luo, H. Q., Fang, L. & Wen, H. H. (2009). *Supercond. Sci. Technol.* **22**, 065003.

Liu, J., Li, F. H., Wan, Z. H., Fan, H. F., Wu, X. J., Tamura, T. & Tanabe, K. (1998). *Mater. Trans. JIM*, **39**, 920–926.

Liu, J., Li, F. H., Wan, Z. H., Fan, H. F., Wu, X. J., Tamura, T. & Tanabe, K. (2001). *Acta Cryst.* A**57**, 540–547.

Lu, B., Li, F. H., Wan, Z. H., Fan, H. F. & Mao, Z. Q. (1997). *Ultramicroscopy*, **70**, 13–22.

Luo, H., Fang, L., Mu, G. & Wen, H.-H. (2007). *J. Cryst. Growth*, **305**, 222–227.

Matsui, Y. & Horiuchi, S. (1988). *Jpn. J. Appl. Phys.* **27**, L2306–L2309.

Montanari, E., Righi, L., Calestani, G., Migliori, A., Gilioli, E. & Bolzoni, F. (2005). *Chem. Mater.* **17**, 1765–1773.

Palatinus, L., Dušek, M., Glaum, R. & El Bali, B. (2006). *Acta Cryst.* B**62**, 556–566.

Palatinus, L., Jacob, D., Cuvillier, P., Klementová, M., Sinkler, W. & Marks, L. D. (2013). *Acta Cryst.* A**69**, 171–188.

Rutzinger, D., Doert, T. & Ruck, M. (2009). *Acta Cryst.* B**65**, 519–526.

Saxton, W. O. (1978). *Computer Techniques for Image Processing in Electron Microscopy.* New York: Academic Press.

Scherzer, O. (1949). *J. Appl. Phys.* **20**, 20–29.

Schiske, P. (1968). *Proceedings of the Fourth European Conference on Electron Microscopy*, pp. 145–146. Rome: Vatican Polyglot Press.

Sha, B. D., Fan, H. F. & Li, F. H. (1993). *Acta Cryst.* A**49**, 877–880.

Torardi, C. C., Subramanian, M. A., Calabrese, J. C., Gopalakrishnan, J., McCarron, E. M., Morrissey, K. J., Askew, T. R., Flippen, R. B., Chowdhry, U. & Sleight, A. W. (1988). *Phys. Rev. B*, **38**, 225.

Van Dyck, D., Lichte, H. & vanderMast, K. D. (1996). *Ultramicroscopy*, **64**, 1–15.

Wang, H. B., Jiang, H., Li, F. H., Che, G. C. & Tang, D. (2002). *Acta Cryst.* A**58**, 494–501.

Wei, F., Baikie, T., An, T., Schreyer, M., Kloc, C. & White, T. J. (2011). *J. Am. Chem. Soc.* **133**, 15200–15211.

Willhammar, T., Sun, J., Wan, W., Oleynikov, P., Zhang, D., Zou, X., Moliner, M., Gonzalez, J., Martínez, C., Rey, F. & Corma, A. (2012). *Nat. Chem.* **4**, 188–194.

Withers, R. L., Schiemer, J., Bourgeois, L., Norén, L. & Liu, Y. (2010). *J. Phys. Conf. Ser.* **226**, 012015.

Wolff, P. M. de (1974). *Acta Cryst.* A**30**, 777–785.

Zou, X. D. & Hovmöller, S. (2003). *Progress in Transmission Electron Microscopy*, pp. 239–277. Berlin: Springer.